12-16-2010

Critical Analysis on the Structural and Magnetic Properties of Bulk and Nanocrystalline Cu-Fe-O

D. Paul Joseph
Materials Science Centre, Department of Nuclear Physics, University of Madras, Guindy Campus, Chennai 600 025, India; Center for Condensed Matter Sciences, National Taiwan University, Taipei Taiwan

C. Venkateswaran
Materials Science Centre, Department of Nuclear Physics, University of Madras, Guindy Campus, Chennai 600 025, India

R. Selva Vennila
Center for Study of Matter at Extreme Conditions, Florida International University, Miami, FL; Lawrence Berkeley National Laboratory, Advanced Light Source, Berkeley, CA

Recommended Citation
D. Paul Joseph, C. Venkateswaran, and R. Selva Vennila, "Critical Analysis on the Structural and Magnetic Properties of Bulk and Nanocrystalline Cu-Fe-O," Advances in Materials Science and Engineering, vol. 2010, Article ID 715872, 14 pages, 2010. doi:10.1155/2010/715872

Hindawi Publishing Corporation
Advances in Materials Science and Engineering
Volume 2010, Article ID 715872, 14 pages
doi:10.1155/2010/715872

Research Article

Critical Analysis on the Structural and Magnetic Properties of Bulk and Nanocrystalline Cu-Fe-O

D. Paul Joseph,[1,2] C. Venkateswaran,[1] and R. Selva Vennila[3,4]

[1] *Materials Science Centre, Department of Nuclear Physics, University of Madras, Guindy Campus, Chennai 600 025, India*
[2] *Center for Condensed Matter Sciences, National Taiwan University, Taipei 10617, Taiwan*
[3] *Center for Study of Matter at Extreme Conditions, Florida International University, Miami, FL 33199, USA*
[4] *Lawrence Berkeley National Laboratory, Advanced Light Source, Berkeley, CA 94720, USA*

Correspondence should be addressed to C. Venkateswaran, cvunom@hotmail.com

Received 1 November 2010; Accepted 16 December 2010

Academic Editor: Jacques Huot

Nanocrystalline and bulk samples of "Fe"-doped CuO were prepared by coprecipitation and ceramic methods. Structural and compositional analyses were performed using X-ray diffraction, SEM, and EDAX. Traces of secondary phases such as $CuFe_2O_4$, Fe_3O_4, and α-Fe_2O_3 having peaks very close to that of the host CuO were identified from the Rietveld profile analysis and the SAED pattern of bulk and nanocrystalline $Cu_{0.98}Fe_{0.02}O$ samples. Vibrating Sample Magnetometer (VSM) measurements show hysteresis at 300 K for all the samples. The ferrimagnetic Neel transition temperature (T_N) was found to be around 465°C irrespective of the content of "Fe", which is close to the T_N value of cubic $CuFe_2O_4$. High-pressure X-Ray diffraction studies were performed on 2% "Fe"-doped bulk CuO using synchrotron radiation. From the absence of any strong new peaks at high pressure, it is evident that the secondary phases if present could be less than the level of detection. Cu_2O, which is diamagnetic by nature, was also doped with 1% of "Fe" and was found to show paramagnetic behavior in contrast to the "Fe" doped CuO. Hence the possibility of intrinsic magnetization of "Fe"-doped CuO apart from the secondary phases is discussed based on the magnetization and charge state of "Fe" and the host into which it is substituted.

1. Introduction

Oxides such as ZnO, TiO_2, and SnO_2 are currently explored as host materials for preparing Diluted Magnetic Semiconductors (DMSs) [1–7]. Among these, diamagnetic ZnO (n-type) doped with "3d" transition metal ions is presently explored in detail ([8–13] and references there in). Wide controversies exist in literature reports in explaining the observed results, and the role of preparation methods in deciding the property. CuO (Tenorite), a p-type semiconductor with a band gap of 1.2 eV, is an essential component in a variety of oxide superconductors and is also known for its catalytic and gas sensing properties [14–16]. CuO also being nontoxic and abundant, an attempt has been made to unravel its properties by doping with "Fe" and to find its potential for application in SPINTRONICS. "Cu" has three oxidation states, Cu^+, Cu^{2+}, and Cu^{3+}, because of which both hole doping and electron doping are possible. "Fe" doping into CuO has been attempted by researchers [17–21] by different preparation methods and was found to have no definite evidence for "Fe" replacing the "Cu" site in CuO, as the two components are immiscible. Smith et al. have reported that introducing Fe_2O_3 into CuO by ceramic method is tough and phase segregation results above 0.3% of "Fe" in CuO [17]. Few reports exist on CuO doped with "Mn" [22] and "Fe" [23, 24] from DMS point of view. On the other hand, Cu_2O (cuprite), also an eco-friendly p-type semiconductor with a direct band gap value of 2 eV [25], is useful as an energy converter for solar cell applications [26] and as humidity and gas sensor material [27, 28]. Reports also exist on magnetic properties of "Mn-", "Co-" and "Fe-" doped Cu_2O [25, 29, 30]. Comparison of "Fe-doped Cu_2O" with "Fe-doped CuO" may throw some light on the understanding of the intrinsic magnetic contribution of the later.

In this work, paramagnetic CuO (antiferromagnetic below 230 K) doped with varying concentration of "Fe"

was characterized in detail for its structural, compositional, and magnetization behavior by X-Ray diffraction (XRD), Rietveld analysis, Scanning electron microscopy (SEM), Energy Dispersive X-Ray analysis (EDAX), Transmission Electron Microscopy (TEM), Vibrating Sample Magnetometer (VSM), Thermogravimetric analyzer (TGA), Mössbauer spectroscopy, and XRD at high-pressures using synchrotron radiation. Presence of other related phases like $CuFe_2O_4/Fe_3O_4$ and Fe_2O_3, having coincidence with many of the major peak positions of CuO, was not categorized before through the powder X-ray diffraction in detail. Their presence is only discussed based on the Mössbauer spectra [20, 21, 23]. We performed a detailed powder X-ray diffraction study using Rietveld refinement procedure and cross checked the presence of $CuFe_2O_4$ from the Neel temperature (T_N) measurement using a TGA with a small applied field. High-pressure studies were carried out to identify the presence of any possible secondary phases. We have also discussed the effect of secondary phases in CuO and also compared with 1% and 2% "Fe"-doped Cu_2O. The possibility of intrinsic magnetization of "Fe"-doped CuO [24] apart from the ferrite phases is discussed based on the magnetization measurements and the charge state of "Fe" in the host into which it is substituted.

2. Sample Preparation and Experimental Details

Nanocrystalline samples of $Cu_{(1-x)}Fe_xO$ (x = 0.01, 0.02, 0.03, 0.04, and 0.05) were prepared from the stoichiometric solutions of copper nitrate and iron nitrate in deionized water by coprecipitation method after refluxing for 20 hour, 30 hour, 40 hour and 50 hour. Precipitation was done using aqueous NH_4OH and peptized with deionized water to remove by-products. The filtrates were then dried, powdered and annealed at various temperatures. Nanocrystalline $CuFe_2O_4$ and bulk $Cu_{(1-x)}Fe_xO$ (x = 0.01, 0.02, 0.03, 0.04, 0.05 and 0.07) were also prepared for comparing the properties. For the preparation of bulk samples, stoichiometric mixtures of oxides were ground in isopropyl alcohol medium, pelleted and sintered at 900°C/12h in air.

Chemical coprecipitation method with subsequent reduction of the precipitates was employed to prepare the samples of Cu_2O : Fe (1% and 2%). Copper sulphate and ferric nitrate solutions for the required stoichiometry were prepared with de-ionized water. Aqueous NH_4OH (0.15 M) solution was added to the solution with constant stirring. After stirring for 15 minutes, 1.2 M NaOH solution was added in drops to the solution, to form light green precipitates. Further, 2 mL of 10 M N_2H_4 was added, continued by 5 hour stirring to reduce the sample to form "Fe"-doped Cu_2O [30] and Cu_2O [31].

2.1. X-Ray Diffraction Results. Nanocrystalline $Cu_{0.95}Fe_{0.05}O$ samples were annealed at 500°C, 700°C, 900°C/2h, and also at 900°C/12h in air. X-Ray diffraction measurements were done using CuK_α radiation in the range 10°–80° with a step size of 0.04° (Rich Seifert 2000, transmission geometry). All the peaks could be indexed to the monoclinic structure of CuO. Representative XRD patterns of 50 hours refluxed $Cu_{0.95}Fe_{0.05}O$ sample annealed at different temperatures are shown in Figure 1. The samples annealed at 700°C/2h presented Fe_2O_3 peaks of small intensity around 31° and 33°. However, after annealing the samples at 900°C those peaks vanished and only lines of CuO phase were evident. Hence all the nanocrystalline $Cu_{(1-x)}Fe_xO$ (x = 0.01, 0.02, 0.03, 0.04, and 0.05) samples and $Cu_{0.95}Fe_{0.05}O$ samples refluxed for 20 hour, 30 hour, 40 hour, and 50 hour were annealed at 900°C/2h. Based on these results the samples were first considered as single phase and the magnetization and other measurements were performed. However, most of the reflections of monoclinic CuO (Monoclinic, JCPDS # 65-2309) match with those of ferrimagnetic $CuFe_2O_4$ (Cubic, JCPDS file No. 77-0010), Fe_3O_4 (Cubic, JCPDS file No. 85-1436), and paramagnetic Fe_2O_3 (Rhombohedral, JCPDS file No. 80-2377). Some of the peaks of $CuFe_2O_4/Fe_3O_4$ and Fe_2O_3 having same hkl planes and position very close to that of the host CuO are tabulated in Table 1. This overlap of reflections presented the problem of identifying hidden impurity phases.

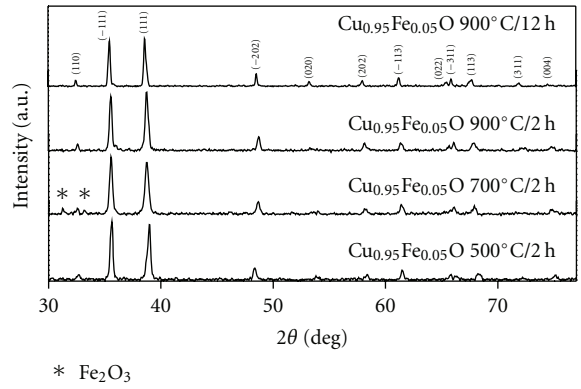

Figure 1: XRD patterns of 50-hour refluxed nanocrystalline $Cu_{0.95}Fe_{0.05}O$ annealed at different temperatures.

2.2. Rietveld Analysis. XRD measurement with a step size of 0.01° with an exposure time of 8 seconds was performed on the as-mixed powders of CuO : Fe_2O_3 (2%) and on the same mixtures but sintered at 900°C/12h in air. Interestingly, from the close scan XRD spectrum, the subtle merged peaks belonging to the ferrimagnetic cubic $CuFe_2O_4$ phase were identified. The full-scale view of the close scan XRD pattern of as-mixed CuO : Fe_2O_3 (2%) presents peaks of CuO and Fe_2O_3. On sintering at 900°C/12h in air, all the lines of Fe_2O_3 vanished indicating the substitution of "Fe" into the copper site and the CuO main phase lines were alone evident. The phase quantification by Rietveld refinement using a program called MAUD [32], which combines the Rietveld method and a Fourier transform analysis, also indicated the existence of 0.2% of $CuFe_2O_4$ in the samples. The results of refinement are given in Table 2. The observed pattern matches with that

Table 1: Peak position, intensity, and hkl values of possible secondary phases in Fe-doped CuO from XRD pattern.

CuO		$CuFe_2O_4$			Fe_3O_4			Fe_2O_3	
2θ	Int	2θ	Int	hkl	2θ	Int	hkl	2θ	Int
35.663	999	35.543	999	311	35.443	999	3 1 1	35.631	719
46.401	14	47.299	009	331	47.162	007	3 3 1	—	—
53.615	71	53.596	076	422	53.438	088	4 2 2	54.066	427
56.863	06	57.135	259	511	56.964	281	5 1 1	—	—
65.989	96	65.974	010	531	65.770	009	5 3 1	66.030	003
75.235	35	75.244	027	622	75.002	030	6 2 2	75.456	059
87.103	09	87.051	022	642	86.754	030	6 4 2	—	—
90.064	15	89.964	081	731	89.650	102	7 3 1	—	—

Table 2: Structural and compositional parameters of bulk as-mixed and sintered $CuO : Fe_2O_3$ (2%) along with possible secondary phases from Rietveld Refinement of the X-ray data.

	$CuO : Fe_2O_3$ (2%)	
Phase	As-mixed	Sintered (900°C/12h in air)
CuO	$a = 4.694$ Å	$a = 4.688$ Å
	$b = 3.433$ Å	$b = 3.425$ Å
Monoclinic (C2/C)	$c = 5.144$ Å	$c = 5.134$ Å
	$\beta = 99.43$	$\beta = 99.47$
	% of CuO = 97.3%	% of CuO = 99.8%
Fe_2O_3	$a = 5.034$ Å	—
Trigonal ($R\bar{3}C$)	$c = 13.802$ Å	
	% of $Fe_2O_3 = 2.7\%$	
$CuFe_2O_4$	—	$a = 8.388$ Å
Cubic ($Fd\bar{3}m$)		% of $CuFe_2O_4 = 0.2\%$
Overall R factor	8.038	1.760
Overall goodness of the fit (σ)	1.223	2.643

of the monoclinic CuO phase there by indicating that the dopants were incorporated into the CuO matrix. The profile analysis and the difference pattern of as-mixed and sintered $CuO : Fe_2O_3$ (2%) along with the vertical lines indicating the peak position of the CuO main phase and the $CuFe_2O_4$ impurity phase are shown in Figure 2. The square root of intensity is plotted so as to clearly depict the closeness of the peaks and also to show the presence of less intense impurity peaks.

2.3. SEM and EDAX Results. SEM measurements were performed on nanocrystalline $Cu_{0.95}Fe_{0.05}O$ samples obtained after refluxing for 40 hour. The image corresponding to the as-prepared sample shows particles with rod-like and disc-shaped morphologies (Figure 3), and their thickness increases when annealed at 500°C/2h in air; however it was less than a micrometer. The thickness and length of the rod shaped particles alone were measured. A Gaussian fit was given and the average value of thickness was found to be 78 nm with an average length of 0.366 μm. As the temperature was raised to 700°C/2h, the rod-like morphology vanishes and the particles grow in size. At 900°C/2h the particle morphology transforms to platelets due to temperature-induced agglomeration and growth (not shown here). Compositional analysis by EDAX confirmed the desired composition of "Fe" in the entire batch of samples (not presented here). The nominal variation in composition is due to the random alloying of the magnetic dopants.

The observation of two different particle morphologies, rod-like and platelet-like may be an indication of existence of two different phases. Rod- and platelet-like morphology may be the undoped CuO and $CuFe_2O_4$ phases, respectively. This argument is supported by the magnetization results which are discussed in the following sections. The samples annealed at lower temperature are found to have paramagnetic component [24] without saturation superimposed with the hysteresis behavior (bottom inset of Figure 10). This is because the temperature is not sufficient for the $CuFe_2O_4$ to crystallize out. Hence, after annealing at 900°C in air, the magnetization curve becomes smooth and the corresponding SEM micrograph presented only platelet-like particles (not presented here).

2.4. TEM Results. The selected area electron diffraction (SAED) on bulk $Cu_{0.95}Fe_{0.05}O$ (900°C/12h) was performed by selecting samples from three different locations in a JEOL EX2000. The TEM micrograph and SAED pattern (inset) is shown in Figure 4. All the d_{hkl} values corresponding to the streaky spot pattern were calculated and compared with the d_{hkl} values of the host CuO (JCPDS 65-2309), and possible secondary phases such as cubic $CuFe_2O_4$ (JCPDS 77-0010), cubic Fe_3O_4 (JCPDS 85-1436), and rhombohedral α-Fe_2O_3 (JCPDS 80-2377). The d_{hkl} and corresponding hkl values of $Cu_{0.95}Fe_{0.05}O$ and possible secondary phases are listed in Table 3. This is also confirmed from SAED patterns for samples taken from three different locations (not shown here). From the above result, it is seen that $Cu_{0.95}Fe_{0.05}O$ sample has the secondary phases of $CuFe_2O_4/Fe_3O_4$ and α-Fe_2O_3.

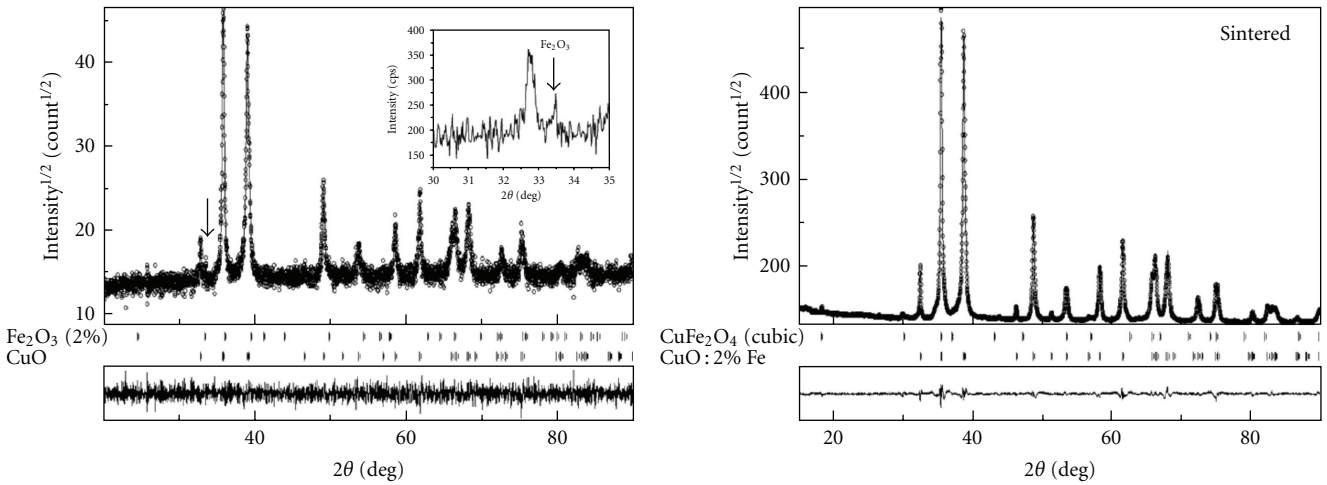

Figure 2: Rietveld refinement of the XRD patterns of as-mixed $CuO : Fe_2O_3$ (2%) (a) and that sintered at 900°C/12h in air (b). The open circles indicate the observed pattern, and the overlying continuous line represents the calculated pattern. The vertical lines indicate the peak position of the respective phases. The bottom continuous line of each pattern represents the difference between the observed and calculated (Obs-Cal) patterns.

Table 3: d_{hkl} and hkl values of bulk $Cu_{0.95}Fe_{0.05}O$ shown in comparison with possible secondary phases to indicate the closeness of the d_{hkl} values.

d_{hkl} (Å) of $Cu_{0.95}Fe_{0.05}O$ from SAED	Monoclinic CuO JCPDS 65-2309		Cubic $CuFe_2O_4$ JCPDS 77-0010		Cubic Fe_3O_4 JCPDS 85-1436		Rhombohedral α-Fe_2O_3 JCPDS 80-2377	
	d_{hkl} (Å)	hkl	d_{hkl} (Å)	hkl	d_{hkl} (Å)	hkl	d_{hkl} (Å)	hkl
2.823	2.742	1 1 0	2.959	2 2 0	2.967	2 2 0	2.699	1 0 4*
2.430	2.515	−1 1 1*	2.523	3 1 1*	2.530	3 1 1*	2.517	1 1 0
2.240	2.315	1 1 1	—	—	—	—	2.206	1 1 3
1.929	1.955	−1 1 2	1.920	3 3 1	1.925	3 3 1	1.841	0 2 4
1.666	1.708	0 2 0	1.610	5 1 1	1.615	5 1 1	1.694	1 1 6
1.485	1.575	2 0 2	1.479	4 4 0	1.483	4 4 0	1.486	2 1 4
1.333	1.371	2 2 0	1.323	6 2 0	1.325	6 2 0	1.349	2 0 8
1.220	1.298	3 1 1	1.208	4 4 4	1.211	4 4 4	1.258	2 2 0
1.109	1.117	−4 0 2	1.118	6 4 2	1.121	6 4 2	1.103	2 2 6
1.015	1.014	2 2 3	1.089	7 3 1	1.092	7 3 1	—	—
0.944	0.941	−1 3 3	—	—	—	—	—	—
0.909	0.915	−3 3 1	—	—	—	—	—	—
0.887	0.888	−3 3 2	—	—	—	—	—	—
0.849	0.851	5 1 1	—	—	—	—	—	—
0.797	0.798	5 1 2	—	—	—	—	—	—

*Indicates the respective 100% peak.

The TEM micrograph of nanocrystalline $Cu_{0.95}Fe_{0.05}O$ (900°C/2h) shown in Figure 5 has agglomerates of smaller particles due to annealing of the sample. The SAED pattern (inset of Figure 5) shows well-defined spots indicating formation of highly crystalline particles on annealing. The d_{hkl} and hkl values are tabulated in Table 4. All the d_{hkl} values match with those of the parent CuO except for the 3.310 Å d_{hkl}, which has good coincidence with that of (012) plane of α-Fe_2O_3. Hence the nanocrystalline $Cu_{0.95}Fe_{0.05}O$ sample also has the possible secondary phases as observed in the SAED of bulk $Cu_{0.95}Fe_{0.05}O$. The equation representing the sample formation with possible secondary phases is given as follows:

$$CuO + Fe_2O_3 \xrightarrow[\Delta]{900^\circ C/12h} Cu_{(1-x)}Fe_xO + CuFe_2O_4(\text{cubic}) + Fe_2O_3\ (\text{Rhombohedral}) + CuO. \quad (1)$$

Table 4: d_{hkl} and hkl values of nanocrystalline $Cu_{0.95}Fe_{0.05}O$ shown in comparison with possible secondary phases to indicate the closely situated d_{hkl} planes.

d_{hkl} (Å) of $Cu_{0.95}Fe_{0.05}O$ from SAED	Monoclinic CuO JCPDS 65-2309		Cubic $CuFe_2O_4$ JCPDS 77-0010		Cubic Fe_3O_4 JCPDS 85-1436		Rhombohedral α-Fe_2O_3 JCPDS 80-2377	
	d_{hkl} (Å)	hkl	d_{hkl} (Å)	hkl	d_{hkl} (Å)	hkl	d_{hkl} (Å)	hkl
3.310	—	—	—	—	—	—	3.682	0 1 2
2.685	2.515	−1 1 1*	2.523	3 1 1*	2.530	3 1 1*	2.699	1 0 4*
2.341	2.315	1 1 1	2.416	2 2 2	2.422	2 2 2	2.517	1 1 0
2.086	1.955	−1 1 2	2.092	4 0 0	2.098	4 0 0	2.078	2 0 2
1.891	1.859	−2 0 2	1.920	3 3 1	1.713	4 2 2	1.841	0 2 4
1.684	1.708	0 2 0	1.708	4 2 2	1.615	5 1 1	1.694	1 1 6
1.616	1.617	0 2 1	1.610	5 1 1	1.483	4 4 0	1.602	1 2 2
1.514	1.501	−1 1 3	1.479	4 4 0	1.418	5 3 1	1.486	2 1 4
1.368	1.375	1 1 3	1.414	5 3 1	1.327	6 2 0	1.349	2 0 8
1.217	1.257	−2 2 2	1.208	4 4 4	1.279	5 3 3	1.213	2 2 3
1.053	1.070	1 3 1	1.089	7 3 1	1.092	7 3 1	1.103	2 2 6
0.917	0.951	−3 3 1	—	—	—	—	—	—
0.748	—	—	—	—	—	—	—	—
0.636	—	—	—	—	—	—	—	—

*Indicates the respective 100% peak.

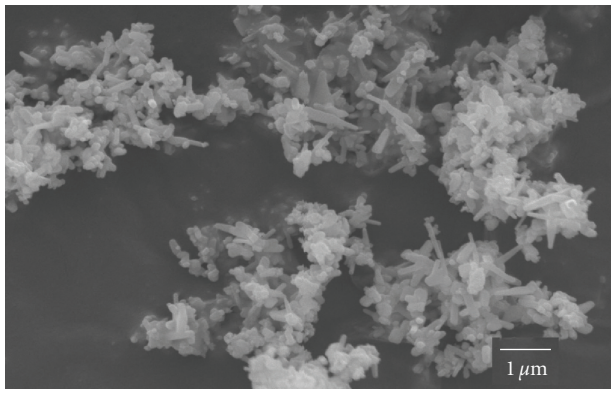

Figure 3: SEM micrograph of 40-hour refluxed nanocrystalline $Cu_{0.95}Fe_{0.05}O$ showing the mixture of rod-like and platelet-like particles.

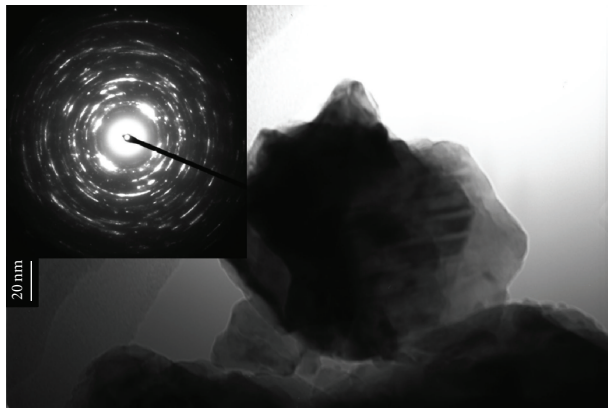

Figure 4: TEM micrograph and SAED pattern of bulk $Cu_{0.95}Fe_{0.05}O$ (900°C/12h).

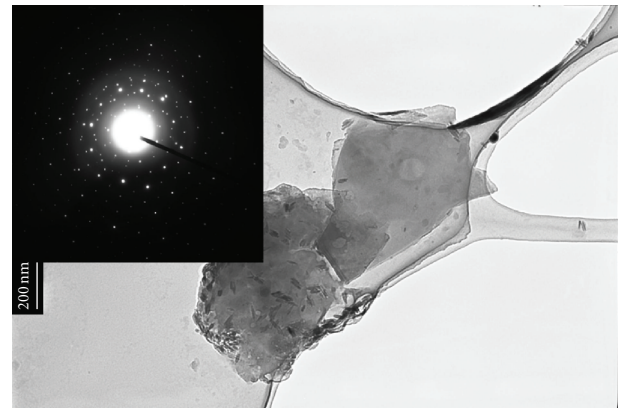

Figure 5: TEM micrograph and SAED pattern of nanocrystalline $Cu_{0.95}Fe_{0.05}O$ (900°C/2h).

2.5. High-Pressure X-Ray Diffraction Using Synchrotron Radiation. Pressure is a fundamental thermodynamic degree of freedom available for basic investigations as well as for processing of materials. The effects of pressure are a result of changes in the band structure and of the energy content of a material produced by the reduction of inter atomic spacing. The study of the behavior of materials at high-pressures has been useful in the observation of new features of the physical and chemical properties. In order to produce appreciable effects on the properties of condensed phases, high-pressures of the order of hundreds or thousands of bars are required. Synchrotron radiation is a photon light source generated by high-energy electrons that are centripetally accelerated to relativistic velocities in the magnetic fields of a storage ring and are emitted in a narrow cone tangent to the orbit. Synchrotron radiation,

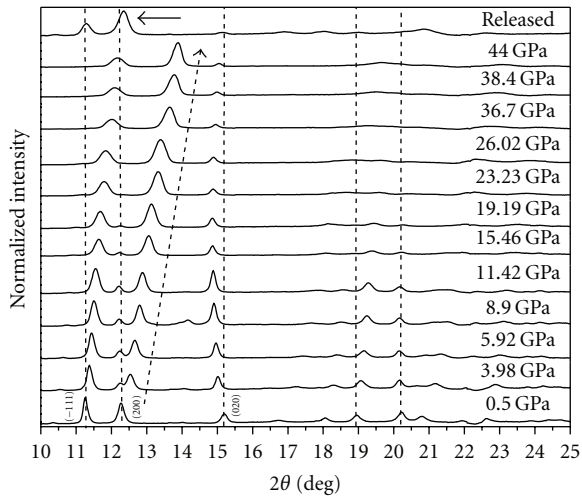

Figure 6: The XRD pattern of the 2% Fe-doped bulk CuO sample at different pressures using synchrotron radiation of wavelength 0.4564 Å.

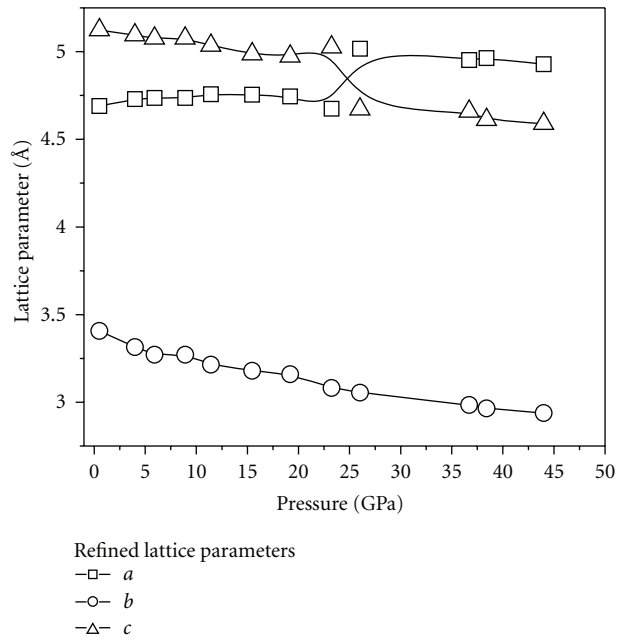

Figure 7: Variation of lattice parameters with pressure of 2% Fe-doped bulk CuO sample. The error in the lattice parameters is equivalent to the size of the markers.

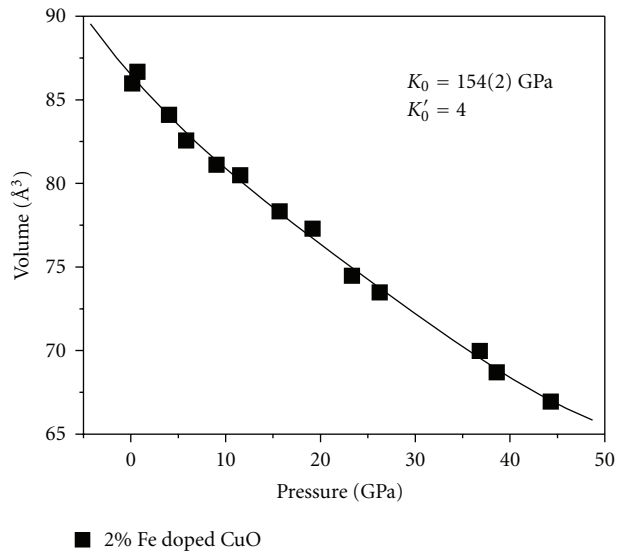

Figure 8: The 3rd-order BM-eos fit without any constraint on K_0' for the 2% Fe-doped bulk CuO sample. The error in the sample volume is equivalent to the size of the markers.

because of unique properties like high brightness, wide energy spectrum, high degree of polarization, and high collimation has allowed extensive investigation of a variety of materials. The remarkable qualities of diamond such as high yield strength and transparency to radiation over a wide range of wavelengths have made it an obvious choice for the anvil materials making it possible to conduct high-pressure X-ray diffraction measurements on materials at few hundreds of giga Pascal (GPa) using synchrotron radiation. Presence of secondary phases can be evidenced from the high-pressure X-ray diffraction measurements due to the fact that the elastic properties of CuO, Fe, and $CuFe_2O_4$ are different. Hence, we are motivated to study the sample at high-pressures to identify the presence of any hidden secondary phases.

High-Pressure XRD measurements were conducted in angle dispersive geometry using Mao-Bell type Diamond Anvil Cell. Experiment was performed using the synchrotron source at beamline 16IDB, High-Pressure Collaboration Access Team (HPCAT), Advanced photon source, Chicago, with a wavelength of 0.4564 Å. Bulk CuO : Fe (2%) powder was loaded along with a few grains of platinum which acts as a pressure standard [33]. A stainless steel gasket of 50 μm thickness indented using diamond anvils of culet size 300 μm, wherein a 100 μm hole drilled serves as the sample chamber. The size of the incident beam was $10 \times 10\,\mu m^2$ and the diffracted beam was recorded on a Mar 3450 image plate. The diffraction measurements were carried out from 0.5 GPa to 44 GPa at room temperature and are shown in Figure 6. Each pattern was fitted and refined to monoclinic structure of CuO with space group $C2_1/c$ using the software GSAS [34] with EXPGUI [35]. Though no structural transitions had been reported up to 100 GPa in monoclinic CuO [36–40], the study helps in identifying the hidden phases based on the variation in compressibility.

In the case of 2% Fe-doped CuO, application of pressure causes a shift in the diffraction peaks towards higher angle indicating reduction in cell volume. Relative variation of refined lattice parameters as a function of pressure is shown in Figure 7. The overall trend on application of pressure on the "*b*" and "*c*" lattice parameters is to decrease them with increasing pressure and that "*a*" increases gradually (Figure 7). The cell volume obtained from the refinement is found to decrease with pressure (Figure 8) and no abrupt change is

observed indicating absence of structural transition. Literature reports indicate absence of structural transition from high-pressure electrical resistivity measurements in monoclinic CuO up to 100 GPa [36, 40].

Upon increasing the pressure, at 3.98 GPa, a peak clearly separates out from the (200) plane. Hence, when CuO gets compressed and shifts towards higher angle, an unknown peak becomes evident. With further increasing pressure, we observed that the (-111) peak of monoclinic CuO shifts towards higher angle and tends to overlap with the unknown peak. As the pressure is further increased, the intensity of the unknown peak gradually decreases and completely vanishes at 26.02 GPa before overlapping with the (-111) plane of CuO. Similar behavior has been observed in pure CuO itself (the results will be published elsewhere). Reimann and Syassen [41] observed changes in the Raman modes of pure CuO in high-pressure Raman measurements up to 34 GPa which they explain as the changes in the internal structure parameter. Reimann and Syassen also report Malinowski to observe a structural anomaly in his X-ray diffraction measurement around 10 Gpa (referred as private communication in back reference of [41]). High-pressure neutron diffraction studies by Ehrenberg et al. [38] suggest Jahn Teller type structural distortion seen below 8 GPa in pure CuO. Hence, appearance and suppression of an additional peak in the high-pressure XRD of 2% Fe-doped CuO sample is also characteristic of pure CuO. The phase transformation is similar to Jahn Teller-like distortion which occurs at high-pressure related to the variation of the bond angle with pressure. In addition to this observation, the absence of any other additional peaks evidences absence of secondary phases of them to be present below the limit of detection. The conclusion was drawn based on the variation of the bulk modulus of CuO and various secondary phases.

The (-111) peak which was the maximum intensity peak at 0.5 GPa loses its intensity gradually with increasing pressure, and at the same time, the (200) peak gain intensity. This may be due to the pressure-induced preferred orientation. This small internal structural distortion [37, 38, 41] is found to be reversible upon releasing the pressure. However, there is a slight shift towards higher angle in the peak positions along with broadening, also, after releasing the pressure, the (200) plane becomes the peak with maximum intensity instead of (-111) plane which may be due to the pressure-induced lattice strain and preferred orientation. However, pressure-induced substitution of a fraction of "Fe" at the "Cu" site might have also resulted which can be understood in more detail from high-pressure neutron diffraction measurement which is more sensitive to the magnetic moment of the elements in the sample when performed in the similar pressure range. The PV-equation of state fitted using the third-order Birch-Murnaghan equation of state (BM-eos) is given by

$$P = \frac{3K_0}{2} * \left[\left(\frac{V_0}{V}\right)^{7/3} - \left(\frac{V_0}{V}\right)^{5/3}\right] * \left[1 + \frac{3}{4} * (K_0' - 4) * \left(\left(\frac{V_0}{V}\right)^{2/3} - 1\right)\right], \quad (2)$$

where K_0 is bulk modulus, K_0' is derivative of bulk modulus with pressure, V_0 is zero pressure volume, and V is volume at pressure P. The value of K_0' set to 4 shown in Figure 8 indicates a steady decrease in volume on increasing the pressure with no abrupt change indicating absence of phase transition. Hence, absence of secondary phases is evident from the high pressure XRD data and even if present, it is well below the level of detection.

2.6. TGA Results. To identify the effect of "Fe%" doping on the T_N of the samples, the TGA measurements were performed with a small applied field ($\approx$20 Oe) to determine the T_N as a function of temperature. The measurement was performed in N_2 atmosphere with a heating rate of 10°C/min up to 600°C. For the 50 hour refluxed nanocrystalline $Cu_{0.95}Fe_{0.05}O$ sample, the T_N was found to increase with decreasing crystallite size (Figure 9). The increase in magnetization prior to T_N in the TGA curves observed for $Cu_{0.95}Fe_{0.05}O$ is due to Hopkinson effect which is also reported in the case of $NiFe_2O_4$ [42]. The bulk $Cu_{0.95}Fe_{0.05}O$ had a T_N of 458°C, whereas a T_N of 479°C (900°C/12h) for the 49 nm sample and that of 486°C (900°C/2h) for the 25 nm sample were observed. Thus the decrease in crystallite size increases the T_N. However, this variation of T_N may be due to the size effect of the copper ferrite phase that has formed within the sample. To avoid the effect of particle size on T_N, we studied the bulk samples prepared by ceramic method to trace the original trend of variation of T_N with "Fe" concentration in CuO. The T_N observed for "Fe"-doped CuO bulk samples is shown in Table 5. There was no noticeable trend in the variation of T_N. The T_N remained around 460°C irrespective of the "Fe%", indicating that one major secondary phase had formed within the sample. This T_N value has good coincidence with the T_N of cubic $CuFe_2O_4$, which is 465°C [43], whereas the T_N of cubic Fe_3O_4 is 585°C. This observation is a clear experimental evidence that the observed hysteresis behaviour is from the phase-segregated $CuFe_2O_4$. This confirms that the "Fe" does not get substituted into the substitutional site of CuO even for 1% of "Fe" in CuO to effect any change in the property of CuO; rather it favors the formation of cubic $CuFe_2O_4$ as segregates within the sample whereas Park et al. [24] do not report any ferrite impurity phase; they instead discuss intrinsic ferromagnetic behaviour in 2% "^{57}Fe"-doped CuO mediated by carriers localized around the oxygen vacancies studied by Mössbauer measurements.

For "Fe"-doped bulk CuO, the T_N is found to be around 460°C. The T_N of Fe_3O_4 is 585°C and is higher than the T_N observed for bulk $Cu_{0.95}Fe_{0.05}O$ whereas the T_N of cubic $CuFe_2O_4$ is 465°C [43]. The T_N of bulk CuO doped with Fe to various extents was very close to that of cubic $CuFe_2O_4$. Hence no appreciable variation in T_N was found with varying "Fe" concentration. Hence, even the 1% and 2% "Fe"-doped CuO is inevitably found to possess copper ferrite phase. $CuFe_2O_4$ when quenched or rapidly cooled (from above 760°C), takes cubic structure with $a = 8.37$ Å. If cooled slowly, it attains tetragonal phase with $a = 8.22$ Å and $c = 8.70$ Å [43]. Since all the samples were furnace cooled from

Table 5: Neel transition temperature of bulk CuO with "Fe" doped to various extent and pure $CuFe_2O_4$.

% of "Fe" in CuO	Neel transition temperature (T_N) °C
$Cu_{0.99}Fe_{0.01}O$	463
$Cu_{0.98}Fe_{0.02}O$	464
$Cu_{0.97}Fe_{0.03}O$	456
$Cu_{0.96}Fe_{0.04}O$	480
$Cu_{0.95}Fe_{0.05}O$	458
$Cu_{0.90}Fe_{0.10}O$	481
$CuFe_2O_4$	483

above 900°C, the cubic phase of $CuFe_2O_4$ is predominantly observed. Hence the observed magnetic property for these samples is not fully intrinsic in nature; instead they have a major contribution from the cubic $CuFe_2O_4$phase leading to a "pinned type" composite magnetic material. Similar observation of contribution from $NiFe_2O_4$ phase has also been reported in the case of Fe-doped NiO by Douvalis et al. from Mössbauer measurements [44].

2.7. Magnetization Results. The magnetization measurements were performed in a Vibrating Sample Magnetometer (VSM) (EG and G Princeton Applied Research VSM 4500) at 300 K. The $Cu_{0.95}Fe_{0.05}O$ samples show clear hysteresis behaviour at room temperature (Figure 10) whereas Borzi et al. had observed paramagnetic behaviour from the Mössbauer measurements for "Fe"-doped CuO, at room temperature [23]. Park et al. [24] have reported ferromagnetic hysteresis behavior for annealing above 500°C; however they explain it as intrinsic behavior due to indirect coupling among the Fe^{3+} ions via a localized carrier at oxygen vacancy. Treatment at 500°C is not sufficient to completely crystallize out $CuFe_2O_4$. We could also observe a paramagnetic-like behaviour for the samples annealed at 500°C/2h from VSM (bottom inset of Figure 10) and the loops did not saturate but were found to show hysteresis at room temperature when annealed at 900°C/2h. Hence, after annealing at 900°C in air, the magnetization curve becomes smooth and the corresponding SEM micrograph also presented only platelet-like particles (not shown here). The M_{max} values were found to increase with increasing refluxing hour (top inset of Figure 10) and also found to increase with increasing "Fe%" in nanocrystalline CuO samples refluxed for 50 hour and annealed at 900°C/2h in air (Figure 11). Inset of Figure 11 shows the comparison of the magnetization data of all the samples with pure copper ferrite; note the large difference in magnetization. This may be presumably due to increasing volume fraction of $CuFe_2O_4$ within the samples. The non-saturation of loops may be due to the following reasons: (a) presence of clusters of undoped paramagnetic CuO (at 300 K), and (b) incomplete formation of ferrite secondary phases, which are responsible for the observed dominant magnetic behaviour.

In our case of "Fe"-doped CuO, ferrimagnetic correlations among "Fe^{2+}" atoms substituting the "Cu" site may lead

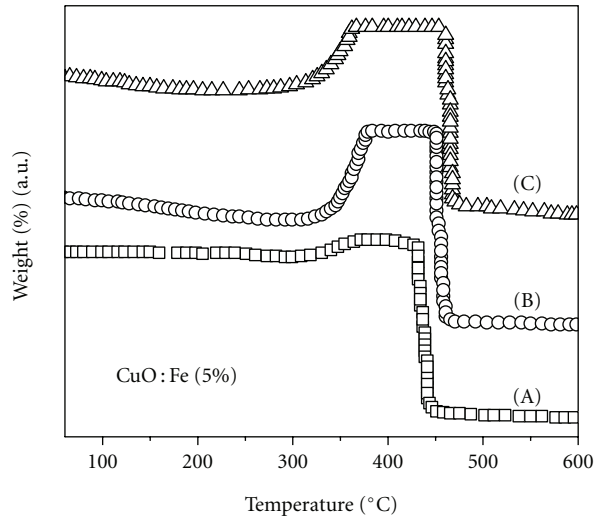

Figure 9: TGA results of samples: (A) bulk $Cu_{0.95}Fe_{0.05}O$, T_N = 458°C, (B) nanocrystalline $Cu_{0.95}Fe_{0.05}O$ annealed at 900°C /12h, T_N = 479°C, (C) nanocrystalline $Cu_{0.95}Fe_{0.05}O$ annealed at 900°C /2h, T_N = 486°C.

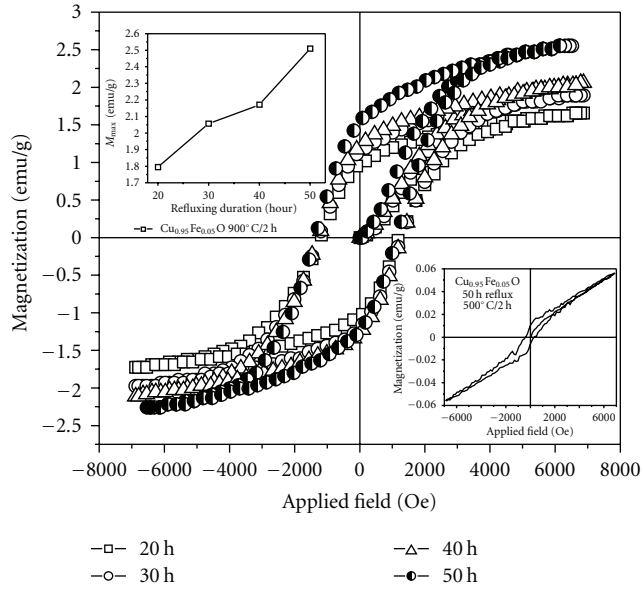

Figure 10: Hysteresis behavior of $Cu_{0.95}Fe_{0.05}O$ refluxed for various durations and annealed at 900°C/2h. Bottom inset represents the paramagnetic behavior of 50 hour refluxed $Cu_{0.95}Fe_{0.05}O$ annealed at 500°C/2h. Top inset represents the increase in M_{max} value with increasing refluxing period.

to an ordered spin configuration enhancing the magnetic susceptibility. But this effect is masked by the dominant ferromagnetic signal from the $CuFe_2O_4$ phase, at 300 K. Though the observed magnetic behavior at 300 K is dominated by the $CuFe_2O_4$ phase, other plausible contribution comes from the "Fe^{2+}" substituted in "Cu" site of CuO. The dominant ferromagnetic signal from $CuFe_2O_4$ masks magnetic contribution from "Fe^{2+}" substituted in CuO and pertains from reaching a conclusive hypothesis. One has to

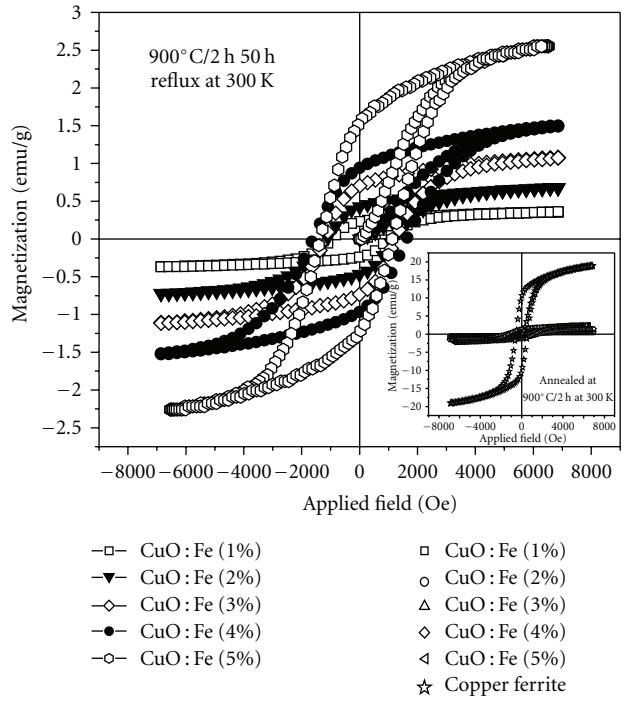

Figure 11: Increase in magnetization (M_{max}) as a function of % of "Fe" in CuO at 300 K for the 50-hour refluxed nanocrystalline sample annealed at 900°C/2h in air. Inset shows the comparison with pure copper ferrite.

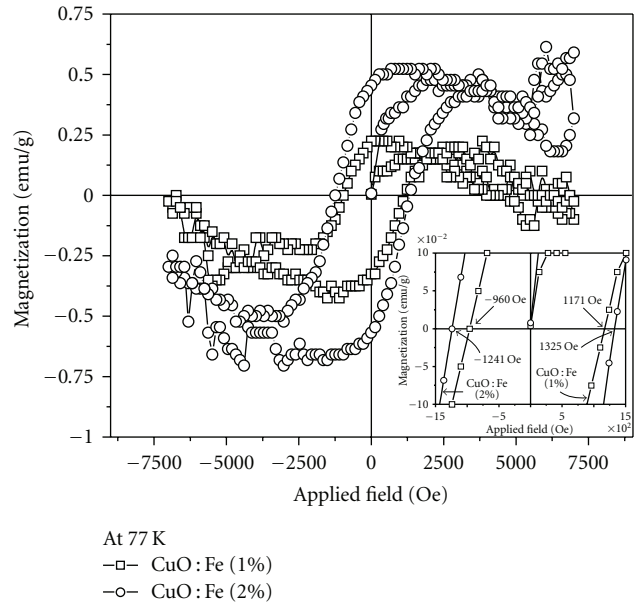

Figure 12: Hysteresis behavior of bulk 1 and 2% "Fe"-doped CuO samples annealed at 900°C/12h in air measured at 77 K. Inset shows the exchange bias behavior.

do more work to explain from the standpoint of "Fe^{2+}" substituting the "Cu" site by delineating the contribution from the segregated $CuFe_2O_4$ phase.

The magnetization measurements on bulk 1% and 2% Fe- doped CuO performed at 77 K showed distorted hysteresis loops (Figure 12). This is because the measurement temperature is well below the Neel temperature (T_N) of CuO. The noncollinear spin arrangement due to partial Fe substitution at the Cu site now weakens and the spin alignment tend towards (perfect anticollinear) antiferromagnetic arrangement. The distorted hysteresis (Figure 12) showed a loop shift away from the $M = 0$ (inset of Figure 12) which is known as exchange bias [45]. Exchange bias is commonly observed in a mixture of antiferromagnetic (AFM) and ferromagnetic (FM) type compounds [46]. Susceptibility studies also show three dimensional AFM behavior below 212 K [47].

The 1% "Fe"-doped CuO showing ferrimagnetic behavior at 300 K is found to present distorted signal at 77 K. At 77 K, CuO is antiferromagnetic; hence the spins tend towards anticollinear arrangement leading to decrease in magnetization. However, if reasonable quantity of $CuFe_2O_4$ is present, then, an increase in magnetization at 77 K should have been observed, but, to the contrary it deteriorates. At 77 K, the sample becomes an antiferromagnetic-ferrimagnetic composite mixture, whereas at 300 K, it is a paramagnetic-ferrimagnetic mixture. At 77 K, the loss of hysteresis behavior could be explained based on the antiferromagnetic transition occurring in CuO in which spins in the anticollinear arrangement dominate by distorting the ferrimagnetic arrangement of $CuFe_2O_4$.

3. Results and Discussion

Based on the above given experimental observations, formation of cubic $CuFe_2O_4$ is confirmed. However one could not discard the candidature of CuO to be an efficient material from applications point of view. This is because, even if $CuFe_2O_4$ phase persists in CuO, the material can be utilized for the fabrication of magnetic tunnel junction (MTJ-) like structures and also there may be an intrinsic magnetic behaviour due to "Fe" substitution in the "Cu" site. The magnetization measurements on CuO, with $CuFe_2O_4$ as an impurity, show large variation in M_{max} and H_C as observed from the magnetization experiments which are essential criteria for an MTJ. There are a reasonable number of literature reports on MTJs composed of partly or all oxide layers. MTJs using Al_2O_3 barrier and an Fe-oxide layer converted to ferromagnetic Fe_3O_4 by annealing have been demonstrated [48]. Heterostructures MTJ device using $Ti_{(1-x)}Co_xO_{(2-\delta)}$ DMS as the spin injection electrode has also been demonstrated [49]. All oxide MTJ's such as $Fe_3O_4/MgO/Fe_3O_4$, $Fe_3O_4/CoCr_2O_4/La_{0.7}Sr_{0.3}MnO_3$ (LSMO) have also been reported [50–53]. In the case of all oxide Fe_3O_4/Mg_2TiO_4 (MTO)/LSMO structure, Alldredge et al. [54] reported minimal mismatch due to similar spinel structure at the Fe_3O_4/MTO interface. They have also reported coercive fields of about 200 and 600 Oe for the LSMO and Fe_3O_4 layers, respectively. Diode effect has been observed in all oxide $Sr_2FeMoO_6/SrTiO_3/CoFe_2O_4$ MTJ by Fix et al. [55]. The coercive field of the two magnetic electrodes in an MTJ should be well separated and the

magnetization reversal of these layers should be abrupt. Hence without attaining single phase one may try to use this material for multilayer switching applications considering it as a composite material of "pinned" type magnetization; the discussion in this point of view is given in this section.

3.1. Pinned Type Composite Magnetic Material. The VSM measurements on CuO doped with varying "Fe%" show the $M_{\max}$ value to increase. Since $CuFe_2O_4$ present in the sample is mainly responsible for the observed magnetic behavior, then with increasing "Fe%" in CuO, the volume fraction of $CuFe_2O_4$ has to increase; that is, the samples should tend towards more soft nature, with high $M_{\max}$ and low H_C. Instead, we observe a linear increase in $M_{\max}$ and an increase in H_C with increasing "Fe%" instead of decrease in H_C (Figure 13) for 1, 4, and 7% "Fe"-doped CuO, which may be due to domain wall pinning effects. The spontaneous magnetic moment per "Fe" atom in CuO for 1, 4, and 7% are 0.0057 μ_B, 0.0168 μ_B, and 0.0276 μ_B, respectively. Besides the enhancement of H_C, the squareness ratio, M_R/M_S also increases with "Fe%" in CuO. The value of squareness ratio of 1, 4 and 7% "Fe" doped CuO is 0.249, 0.448, and 0.519, respectively. This is an indication that the "Fe"-doped CuO tend towards "hard" nature in spite of the presence of soft magnetic $CuFe_2O_4$.

The H_C value of 7% "Fe"-doped bulk CuO (620 Oe) is three times greater than the value of 1% "Fe"-doped bulk CuO (202 Oe) (Figure 13 inset) indicating that the layer of "Fe" composition-varied CuO thin films may show exchange coupling. High H_C CuO layer may be used as a "pinned" layer in MTJ structures. The H_C of bulk and nanocrystalline $Cu_{0.95}Fe_{0.05}O$ was found to be 236 Oe and 1225 Oe, respectively. The H_C increased five times in magnitude in the nanocrystalline sample (Figure 14). The $M_{\max}$ value of nanocrystalline CuO : Fe (1% to 5%) is found to increase with "Fe" concentration (Figure 14 inset). These aspects could induce exchange coupling which is desirable for device fabrication if one could stabilize a single phase Cu–Fe–O solid solution without any ferrite formation by adopting different preparation techniques or by preparing a sample with homogenously dispersed $CuFe_2O_4$ in CuO.

By comparing the virgin magnetization curve in the hysteresis loop, one recognizes two qualitatively different kinds of behavior: (i) nucleation type and (ii) pinning type [56]. In a nucleation type magnet, the virgin curve is steep and saturation is reached under fields much lower than the saturation loop coercive field. Domain walls are present in the virgin state and the fact that the material can be easily saturated shows that walls are free to move and do not experience any important pinning effects. Once the virgin domain structure has been swept away, the formation of reversed domains becomes a difficult process, and the demagnetization curve is characterized by a substantial coercivity.

In a pinning type magnet, fields of the order of the saturation loop coercive field are required to saturate the material even when one starts from the virgin state. This indicates that domain wall pinning is the main mechanism responsible for coercivity. Domain wall motion is

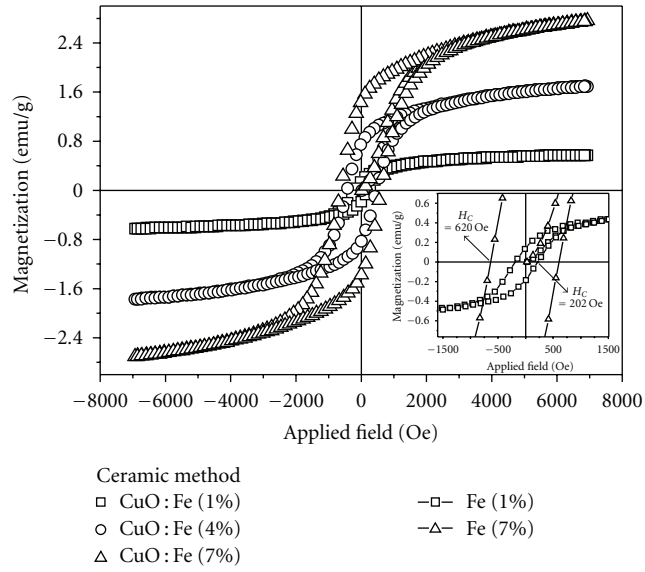

Figure 13: Hysteresis loop of 1%, 4%, and 7% "Fe"-doped bulk CuO at 300 K. Inset shows the large variation in coercivity of 1% and 7% "Fe"-doped samples.

the dominant mechanism and the loop width is mainly determined by wall pinning effects [56]. The impediments to wall motion will determine the coercive field. The physical picture summarized by the term wall pinning is one where the impediments to wall motion arise from some form of structural disorder; dispersed phases with magnetic properties different from those of the matrix, as well as nonmagnetic inclusions or cavities, may also be important sources of pinning. The strength of the pinning effect may critically depend on the dimensionality of the pinning sources. The strength, density, and dimensionality of pinning centers can affect the value of H_C. Though the solubility of "Fe" in CuO is very much limited, a very small quantity of any immiscible component will always dissolve in another component, as this increases the configurational entropy and lowers the free energy of the crystal [57]. Hence, though the formation of $CuFe_2O_4$ is more favorable while trying to dope "Fe" in CuO, a fraction of "Fe" also enters into the Cu^{2+} site as substitutional impurity. Hence contribution from intrinsic magnetization from the fraction of Cu–Fe–O substitutional solid solution formed within the sample apart from the composite like behavior of paramagnetic CuO dispersed with $CuFe_2O_4$ particles cannot be disregarded. Hence, one has to really ascertain its effect delineating the major magnetic contribution from the segregated $CuFe_2O_4$ phase. The intrinsic magnetic behavior could result from the spin alignment induced by the fraction of "Fe" substituting the "Cu" site. One could also argue that as the "Fe%" in CuO increases, the fraction of "Fe" substituting the cationic site also increases reasonably. However to cross check this argument, neutron diffraction measurements at ambient and at high-pressures are necessary.

3.2. Comparison of 1% Fe Doped CuO and Cu_2O. The results of 1% "Fe"-doped Cu_2O imply us to elucidate the role of

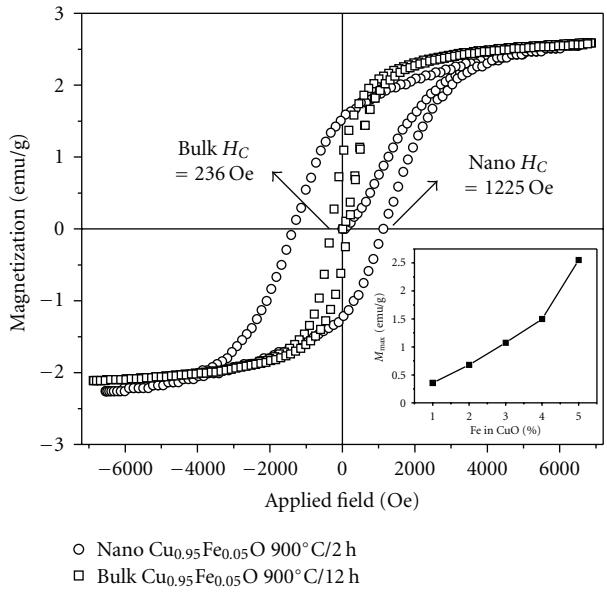

Figure 14: Room temperature hysteresis loops of bulk and nanocrystalline (50 hour refluxed, annealed at 900°/2h) $Cu_{0.95}Fe_{0.05}O$ showing five-fold increase in coercivity. Inset shows the increase in M_{max} value with increasing "Fe" concentration in nanocrystalline samples.

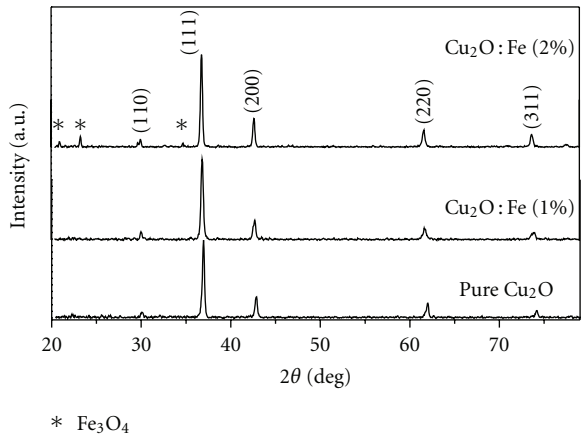

Figure 15: XRD patterns of pure Cu_2O, 1% "Fe"-doped single phase Cu_2O, and 2% "Fe"-doped Cu_2O with impurity peaks of Fe_3O_4.

substitutional "Fe" in CuO. The non-observation of room temperature ferromagnetic behaviour in diamagnetic Cu_2O doped with 1% of "Fe" is another indirect support for the plausible intrinsic magnetization of "Fe"-doped CuO. The XRD pattern of pure Cu_2O ($a = 4.253$ Å) confirmed the cubic structure of Cu_2O and is shown in comparison with 1% and 2% "Fe"-doped Cu_2O in Figure 15. Single phase 1% "Fe"-doped Cu_2O was achieved by optimizing the concentration of N_2H_4 and the stirring duration. The XRD pattern of 2% "Fe"-doped Cu_2O showed secondary phases of Fe_3O_4 which is shown in comparison with pure Cu_2O in Figure 15. The compositional analysis by EDAX confirmed the near stoichiometry of 1% and 2% "Fe"-doped Cu_2O as it is a random alloy. Reproducibility was confirmed by numerous

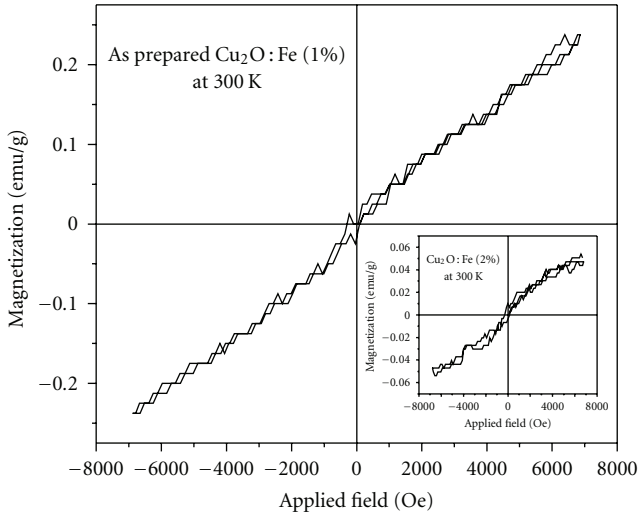

Figure 16: Paramagnetic behavior of 1% Fe-doped Cu_2O at 300 K. Inset shows the same for 2% "Fe"-doped Cu_2O.

trials because formation of Cu_2O by wet chemistry method fairly has a chance of formation of $CuFe_2O_4$ and metallic "Fe" on over reduction with N_2H_4. Moreover the as-prepared samples were crystalline in nature due to preparation by reducing with N_2H_4. Hence annealing was not performed for any of the samples. Moreover, copper (I) oxide, being a meta stable phase, turns into a stable copper (II) oxide when heated above 160°C in air. The magnetization measurements on 1% "Fe"-doped Cu_2O at 300 K showed paramagnetic behavior (Figure 16) [30]. Pure Cu_2O is diamagnetic, but on doping with "Fe", the material exhibits paramagnetic behavior. The low temperature measurements at 77 K show clear diamagnetic behavior (not shown here) indicating the non-ferromagnetic role played by impurities present, if any. The magnetization measurements on 2% "Fe"-doped Cu_2O sample, though having Fe_3O_4 phase, did not show clear room temperature ferromagnetism (Inset of Figure 16), whereas 1% and 2% "Fe"-doped CuO presents clear ferromagnetic hysteresis behavior which suggests possible contribution from Cu–Fe–O in addition to that from cubic $CuFe_2O_4$. Neutron diffraction measurements at ambient and at high-pressures are necessary on both the Fe-doped CuO and Cu_2O samples to shed more light in this aspect.

For the formation of AB_2O_4 spinel structure, A is required to be a dipositive ion, but in Cu_2O, "Cu" is in +1 oxidation state and hence formation of spinel $CuFe_2O_4$ is not favored. Due to the absence of this spinel impurity phase, "Fe" doped Cu_2O does not show a dominant ferromagnetic property as it is observed in the case of 1% Fe-doped CuO.

The coordination number between Cu and O atoms in tenorite CuO (2+) and cuprite Cu_2O (1+) is believed to play a crucial role in the observed difference in their magnetic properties with "Fe" doping. In monoclinic CuO, the Cu atoms are coordinated to four coplanar oxygen situated at the corners of an almost rectangular parallelogram [17] with two more distant apical "O" atoms. A distorted octahedron is formed because of large Jahn-teller effect. Depending on the valence state (1+, 2+ or 3+), a "Fe" ion has up to 5, 4

and "3d" electrons with a total spin of $s = 2\frac{1}{2}$, $s = 2$ and $s = 1\frac{1}{2}$, respectively, due to Hund's rule. A Cu ion has a total spin of 1/2 and hence "Fe" ions doped into CuO have extra moments which are coupled to the lattice of Cu spins via superexchange. CuO at 300 K is paramagnetic and has one unpaired spin due to the $3d^9$ electronic configuration. The fraction of Fe^{3+} ions substituted at the "Cu" sites in CuO has 5 unpaired electrons, which might also contribute to the observed magnetic property of "Fe"-doped CuO by forcing the "Fe" magnetic dipoles to align ferromagnetically by interacting with the unpaired spins of the CuO which is at paramagnetic state at 300 K. Extending the analogy in CuO : Mn [22], we suppose that a fraction of "d" electron states are available for hopping between the "Fe" sites and hence mediating ferromagnetism through the Hund's rule coupling. Hence we attribute the observed magnetic behavior of CuO : Fe to have a dominant hidden intrinsic nature apart from the segregated $CuFe_2O_4$ phase whereas this is not in the case of Cu_2O, where we have Cu^+ ions coordinated linearly to two "O" ions, due to its $3d^{10}$ configuration. There are no unpaired spins and the spin value is s = 0. Hence on substituting with 1% Fe, irrespective of the charge state of "Fe", the Cu_2O matrix could not mediate a ferromagnetic ordering through the substituted "Fe" ions. Hence, the spin configuration of the host matrix into which "Fe" is doped is also responsible for the observed magnetic behavior.

4. Conclusion

The XRD, TEM, and TGA results imply that the observed magnetic properties of "Fe"-doped CuO have contribution from the impurity phases, the nature of variation of H_C and $M_{\max}$ with increasing "Fe%", and the role of substitutional "Fe" and non-observation of ferromagnetic behavior in "Fe"-doped Cu_2O invites exclusive investigation on CuO. Achieving ferromagnetic behavior from a paramagnetic/antiferromagnetic host by creating a spin imbalance seems to be relatively easier and advantageous than achieving it from diamagnetic oxides like ZnO, TiO_2, and so on. The size dependent magnetic properties of "Fe"-doped CuO with controlled formation of $CuFe_2O_4$ are another interesting aspect of this material which could be exploited for applications by suitably varying the size of the particles. The above said properties could be exploited for device applications provided if the "Fe" composition in CuO and the preparatory method and processing conditions are stabilized so as to result in a good single phase Cu–Fe–O solid solution with intrinsic magnetization and high reproducibility. Variation of H_C in "Fe"-doped CuO, though $CuFe_2O_4$ phases are present, extends from "soft" magnetic behaviour to "hard" with variation of "Fe%" in the samples studied. This wide variation in H_C of such a DMS-like composite material could be thought of for fabricating MTJs with low H_C-"free" layer and high H_C-"pinned" layer separated by a thin insulating layer. The advantage of MTJ's made up of such all oxide DMS like layers with high $M_{\max}$, T_N, and H_C over the metallic Fe/AlO_x/NiFe and CoFeB/AlO_x/CoFeB type of MTJs is that these are less complicated and cheap and will have very good lattice matching and least strain between the "pinned" and "free" layers.

Acknowledgments

D. Paul Joseph thanks the CSIR, Government of India, for the award of Senior Research Fellowship, 2007 and Dr. R. Justin Joseyphus, NIT, Trichy, for TEM measurements. The authors thank Prof. Dr. A. Narayansamy of their department and Prof. Dr. M. Palanichamy, Department of Chemistry, Anna University, for critical comments and fruitful discussions. R. S. Vennila acknowledges the Air Force Grant No. 212600548 and COMPRES for the financial support to carry out the above research. Also, the author thanks Prof. S. K. Saxena, Florida International University and Dr. H. P. Liermann of HPCAT (Sector 16), APS, Argonne National Laboratory for their help. Use of the HPCAT facility was supported by DOE-BES, DOE-NNSA (CDAC), NSF, DOD-TACOM, and the W. M. Keck foundation.

References

[1] K. Rode, A. Anane, R. Mattana, J. P. Contour, O. Durand, and R. LeBourgeois, "Magnetic semiconductors based on cobalt substituted ZnO," *Journal of Applied Physics*, vol. 93, no. 10, pp. 7676–7678, 2003.

[2] P. V. Radovanovic and D. R. Gamelin, "High-temperature ferromagnetism in Ni-doped ZnO aggregates prepared from colloidal diluted magnetic semiconductor quantum dots," *Physical Review Letters*, vol. 91, no. 15, Article ID 157202, 4 pages, 2003.

[3] D. P. Joseph, G. S. Kumar, and C. Venkateswaran, "Structural, magnetic and optical studies of $Zn_{0.95}Mn_{0.05}O$ DMS," *Materials Letters*, vol. 59, no. 21, pp. 2720–2724, 2005.

[4] Y. Matsumoto, M. Murakami, T. Shono et al., "Room-temperature ferromagnetism in transparent transition metal-doped titanium dioxide," *Science*, vol. 291, no. 5505, pp. 854–856, 2001.

[5] S. B. Ogale, R. J. Choudhary, J. P. Buban et al., "High temperature ferromagnetism with a giant magnetic moment in transparent co-doped $SnO_{2-\delta}$," *Physical Review Letters*, vol. 91, no. 7, Article ID 077205, 4 pages, 2003.

[6] T. S. Herng, S. P. Lau, S. F. Yu, H. Y. Yang, K. S. Teng, and J. S. Chen, "Enhancement of ferromagnetism and stability in Cu-doped ZnO by N_2O annealing," *Journal of Physics: Condensed Matter*, vol. 19, Article ID 356214, 2007.

[7] S. Deka and P. A. Joy, "Synthesis and magnetic properties of Mn doped ZnO nanowires," *Solid State Communications*, vol. 142, no. 4, pp. 190–194, 2007.

[8] H. Ohno, "Making nonmagnetic semiconductors ferromagnetic," *Science*, vol. 281, no. 5379, pp. 951–956, 1998.

[9] K. Sato and H. Katayama-Yoshida, "Stabilization of ferromagnetic states by electron doping in Fe-, Co- or Ni-doped ZnO," *Japanese Journal of Applied Physics*, vol. 40, no. 4, pp. L334–L336, 2001.

[10] D. P. Joseph, S. Naveenkumar, N. Sivakumar, and C. Venkateswaran, "Synthesis of $Zn_{0.95}Cr_{0.05}O$ DMS by co-precipitation and ceramic methods: structural and magnetization studies," *Materials Chemistry and Physics*, vol. 97, no. 1, pp. 188–192, 2006.

[11] T. Fukumura, Y. Yamada, K. Tamura et al., "Magneto-optical spectroscopy of anatase TiO2 doped with Co," *Japanese Journal of Applied Physics*, vol. 42, no. 2, pp. L105–L107, 2003.

[12] Ü. Özgür, Ya. I. Alivov, C. Liu et al., "A comprehensive review of ZnO materials and devices," *Journal of Applied Physics*, vol. 98, no. 4, Article ID 041301, 103 pages, 2005.

[13] K. Ando, H. Saito, Z. Jin et al., "Magneto-optical properties of ZnO-based diluted magnetic semiconductors," *Journal of Applied Physics*, vol. 89, no. 11, pp. 7284–7286, 2001.

[14] P. Dal, H. A. Mook, G. Aeppll, S. M. Hayden, and F. Doğan, "Resonance as a measure of pairing correlations in the high-Tc superconductor $YBa_2Cu_3O_{6.6}$," *Nature*, vol. 406, no. 6799, pp. 965–968, 2000.

[15] C. L. Carnes and K. J. Klabunde, "The catalytic methanol synthesis over nanoparticle metal oxide catalysts," *Journal of Molecular Catalysis A: Chemical*, vol. 194, no. 1-2, pp. 227–236, 2003.

[16] M. Frietsch, F. Zudock, J. Goschnick, and M. Bruns, "CuO catalytic membrane as selectivity trimmer for metal oxide gas sensors," *Sensors and Actuators B: Chemical*, vol. 65, no. 1, pp. 379–381, 2000.

[17] M. G. Smith, R. D. Taylor, M. P. Pasternak, and H. Oestereicher, "Mössbauer spectroscopy of CuO and its relevance to high-temperature superconductors," *Physical Review B*, vol. 42, no. 4, pp. 2188–2192, 1990.

[18] P. Shah and A. Gupta, "Mössbauer study of iron-doped CuO," *Physical Review B*, vol. 45, no. 1, pp. 483–485, 1992.

[19] S. B. Ogale, P. G. Bilurkar, S. Joshi, and G. Marest, "Ion57 implantation in laser-deposited cupric and cuprous oxide films: Mössbauer spectroscopy and X-ray-diffraction studies," *Physical Review B*, vol. 50, no. 14, pp. 9743–9751, 1994.

[20] A. Gupta and P. Shah, "Effect of oxygen stoichiometry in CuO," *Physical Review B*, vol. 50, no. 18, pp. 13706–13709, 1994.

[21] S. J. Stewart, G. F. Goya, G. Punte, and R. C. Mercader, "Phase transformations in Fe-doped cupric oxide," *Journal of Physics and Chemistry of Solids*, vol. 58, no. 1, pp. 73–77, 1997.

[22] S. G. Yang, T. Li, B. X. Gu et al., "Ferromagnetism in Mn-doped CuO," *Applied Physics Letters*, vol. 83, no. 18, pp. 3746–3748, 2003.

[23] R. A. Borzi, S. J. Stewart, G. Punte et al., "Effect of ion doping on CuO magnetism," *Journal of Applied Physics*, vol. 87, no. 9, pp. 4870–4872, 2000.

[24] Y. R. Park, K. J. Kim, S. L. Choi et al., "Ferromagnetism in Fe-doped cupric oxide," *Physica Status Solidi B*, vol. 244, no. 12, pp. 4578–4581, 2007.

[25] M. Ivill, M. E. Overberg, C. R. Abernathy et al., "Properties of Mn-doped CuO semiconducting thin films grown by pulsed-laser deposition," *Solid-State Electronics*, vol. 47, no. 12, pp. 2215–2220, 2003.

[26] T. Tanaka, "Optical constants of polycrystalline 3d transition metal. Oxides in the wavelength region 350 to 1200 nm," *Japanese Journal of Applied Physics*, vol. 18, no. 6, pp. 1043–1047, 1979.

[27] Y. Ushio, M. Miyayama, and H. Yanagida, "Photoinduced current of CuO/ZnO thin-film heterojunction in humid atmosphere," *Japanese Journal of Applied Physics*, vol. 33, no. 2, pp. 1136–1139, 1994.

[28] D. H. Yoon, J. H. Yu, and G. M. Choi, "CO gas sensing properties of ZnO-CuO composite," *Sensors and Actuators B*, vol. 46, no. 1, pp. 15–23, 1998.

[29] S. N. Kale, S. B. Ogale, S. R. Shinde et al., "Magnetism in cobalt-doped CuO thin films without and with Al, V, or Zn codopants," *Applied Physics Letters*, vol. 82, no. 13, pp. 2100–2102, 2003.

[30] D. P. Joseph, T. P. David, S. P. Raja, and C. Venkateswaran, "Phase stabilization and characterization of nanocrystalline Fe-doped Cu_2O," *Materials Characterization*, vol. 59, no. 8, pp. 1137–1139, 2008.

[31] W. Wang, O. K. Varghese, C. Ruan, M. Paulose, and C. A. Grimes, "Synthesis of CuO and Cu_2O crystalline nanowires using $Cu(OH)_2$ nanowire templates," *Journal of Materials Research*, vol. 18, no. 12, pp. 2756–2759, 2003.

[32] L. Lutterotti, "MAUD materials analysis using diffraction version:1.84," 2002, http://www.ing.unitn.it/~maud/.

[33] N. C. Holmes, J. A. Moriarty, G. R. Gathers, and W. J. Nellis, "The equation of state of platinum to 660 GPa (6.6 Mbar)," *Journal of Applied Physics*, vol. 66, no. 7, pp. 2962–2967, 1989.

[34] A. C. Larson and R. B. von Dreele, "General Structure Analysis System (GSAS)," National Laboratory Report LAUR 86-748, 2004.

[35] B. H. Toby, "EXPGUI, a graphical user interface for GSAS," *Journal of Applied Crystallography*, vol. 34, no. 2, pp. 210–213, 2001.

[36] L. C. Bourne, P. Y. Yu, A. Zettl, and M. L. Cohen, "High-pressure electrical conductivity measurements in the copper oxides," *Physical Review B*, vol. 40, no. 16, pp. 10973–10976, 1989.

[37] A. Malinowski, S. Asbrink, and A. Kvick, "A high-pressure single-crystal X-ray diffraction study of copper oxide using synchrotron radiation," *High Pressure Research*, vol. 4, no. 1, pp. 429–431, 1990.

[38] H. Ehrenberg, J. A. McAllister, W. G. Marshall, and J. P. Attfield, "Compressibility of copper-oxygen bonds: a high-pressure neutron powder diffraction study of CuO," *Journal of Physics Condensed Matter*, vol. 11, no. 34, pp. 6501–6508, 1999.

[39] Z. Wang, V. Pischedda, S. K. Saxena, and P. Lazor, "X-ray diffraction and Raman spectroscopic study of nanocrystalline CuO under pressures," *Solid State Communications*, vol. 121, no. 5, pp. 275–279, 2002.

[40] S. Minomura and H. G. Drickamer, "Effect of pressure on the electrical resistance of some transition-metal oxides and sulfides," *Journal of Applied Physics*, vol. 34, no. 10, pp. 3043–3048, 1963.

[41] K. Reimann and K. Syassen, "Pressure dependence of Raman modes in CuO," *Solid State Communications*, vol. 76, no. 2, pp. 137–140, 1990.

[42] E. C. Stoner and E. P. Wohlfarth, "A mechanism of magnetic hysteresis in heterogeneous alloys," *Philosophical Transactions of the Royal Society A*, vol. 240, pp. 599–642, 1948.

[43] B. D. Cullity, *Introduction to Magnetic Materials*, Addison-Wesley, Philippines, Pa, USA, 1972.

[44] A. P. Douvalis, L. Jankovic, and T. Bakas, "The origin of ferromagnetism in ^{57}Fe-doped NiO," *Journal of Physics Condensed Matter*, vol. 19, no. 43, Article ID 436203, 2007.

[45] A. Punnoose, H. Magnone, M. S. Seehra, and J. Bonevich, "Bulk to nanoscale magnetism and exchange bias in CuO nanoparticles," *Physical Review B*, vol. 64, no. 17, Article ID 174420, 8 pages, 2001.

[46] W. H. Meiklejohn and C. P. Bean, "New magnetic anisotropy," *Physical Review*, vol. 105, no. 3, pp. 904–913, 1957.

[47] T. I. Arbuzova, A. A. Samokhvalov, I. B. Smolyak, B. V. Karpenko, N. M. Chebotaev, and S. V. Naumov, "Temperature transition from 3D to quasi-1D antiferromagnetism in CuO

single crystals," *Journal of Magnetism and Magnetic Materials*, vol. 95, no. 2, pp. 168–174, 1991.

[48] S. Cardoso, Z. Zhang, H. Li et al., "Characterization of nano-oxide layers fabricated by ion beam oxidation," *IEEE Transactions on Magnetics*, vol. 38, no. 5, pp. 2755–2757, 2002.

[49] H. Toyosaki, T. Fukumura, K. Ueno, M. Nakano, and M. Kawasaki, "A ferromagnetic oxide semiconductor as spin injection electrode in magnetic tunnel junction," *Japanese Journal of Applied Physics*, vol. 44, no. 28, pp. L896–L898, 2005.

[50] X. W. Li, A. Gupta, G. Xiao, W. Qian, and V. P. Dravid, "Fabrication and properties of heteroepitaxial magnetite (FeO) tunnel junctions," *Applied Physics Letters*, vol. 73, no. 22, pp. 3282–3284, 1998.

[51] P. A. A. van der Heijden, P. J. H. Bloemen, J. M. Metselaar et al., "Interlayer coupling between FeO layers separated by an insulating nonmagnetic MgO layer," *Physical Review B*, vol. 55, no. 17, pp. 11569–11575, 1997.

[52] P. J. van der Zaag, P. J. H. Bloemen, J. M. Gaines et al., "On the construction of an Fe_3O_4-based all-oxide spin valve," *Journal of Magnetism and Magnetic Materials*, vol. 211, no. 1, pp. 301–308, 2000.

[53] G. Hu, R. Chopdekar, and Y. Suzuki, "Observation of inverse magnetoresistance in epitaxial magnetite/manganite junctions," *Journal of Applied Physics*, vol. 93, no. 10, pp. 7516–7518, 2003.

[54] L. M. B. Alldredge, R. V. Chopdekar, B. B. Nelson-Cheeseman, and Y. Suzuki, "Complex oxide-based magnetic tunnel junctions with nonmagnetic insulating barrier layers," *Journal of Applied Physics*, vol. 99, no. 8, Article ID 08K303, 2006.

[55] T. Fix, D. Stoeffler, Y. Henry et al., "Diode effect in all-oxide Sr_2FeMoO_6-based magnetic tunnel junctions," *Journal of Applied Physics*, vol. 99, no. 8, Article ID 08J107, 2006.

[56] G. Bertotti, *Hysteresis in Magnetism*, chapter 10, 11, Academic Press, New York, NY, USA, 1998.

[57] V. Raghavan, *Materials Science and Engineering*, Prentice-Hall, New Delhi, India, 3rd edition, 1995.

The Scientific World Journal

Hindawi Publishing Corporation
http://www.hindawi.com

Volume 2014